Apparent critical phenomena in the superionic phase transition of $Cu_{2-x}Se$

2016 New J. Phys. 18 013024

(http://iopscience.iop.org/1367-2630/18/1/013024)

New Journal of Physics
The open access journal at the forefront of physics

Deutsche Physikalische Gesellschaft DPG
IOP Institute of Physics

Published in partnership with: Deutsche Physikalische Gesellschaft and the Institute of Physics

OPEN ACCESS

RECEIVED
30 September 2015

REVISED
17 November 2015

ACCEPTED FOR PUBLICATION
16 December 2015

PUBLISHED
11 January 2016

PAPER

Apparent critical phenomena in the superionic phase transition of $Cu_{2-x}Se$

Stephen Dongmin Kang[1,2], Sergey A Danilkin[3], Umut Aydemir[1,2], Maxim Avdeev[3], Andrew Studer[3] and G Jeffrey Snyder[1,2]

[1] Department of Applied Physics and Materials Science, California Institute of Technology, CA 91125, USA
[2] Department of Materials Science and Engineering, Northwestern University, IL 60208, USA
[3] Bragg Institute, Australian Nuclear Science and Technology Organisation, Lucas Heights, NSW 2232, Australia

E-mail: jeff.snyder@northwestern.edu

Keywords: phase transition, superioinic conductors, thermoelectrics, thermopower

Abstract

The superionic phase transition of $Cu_{2-x}Se$ accompanies drastic changes in transport properties. The Seebeck coefficient increases sharply while the electrical conductivity and thermal diffusivity drops. Such behavior has previously been attributed to critical phenomena under the assumption of a continuous phase transition. However, applying Landau's criteria suggests that the transition should be first order. Using the phase diagram that is consistent with a first order transition, we show that the observed transport properties and heat capacity curves can be accounted for and modeled with good agreement. The apparent critical phenomena is shown to be a result of compositional degree-of-freedom. Understanding of the phase transition allows to explain the enhancement in the thermoelectric figure-of-merit that is accompanied with the transition.

1. Introduction

Superionic materials with electrically semiconducting behavior have been shown to be a promising class of thermoelectric materials with a figure-of-merit comparable to those of current state-of-art materials [1–5]. Liquid-like ionic conductivity of cations ($\sigma_i > 1$ S cm^{-1}) in a solid-state, which is referred to as superionic [6], indicates a highly disordered cation sublattice that generally results in a low lattice thermal conductivity [1]. While being thermally insulating, some of these materials exhibit electrical properties that resemble a heavily doped semiconductor. The anion sublattice retains the periodicity of a static crystal, making it somewhat possible to apply a band conduction model. Such combination of electrical and thermal properties in a semiconductor is in fact what is needed for high thermoelectric performance [7], as can be seen from the thermoelectric figure-of-merit defined as:

$$zT = \frac{\sigma_e \alpha^2}{\kappa} T, \tag{1}$$

where α is the Seebeck coefficient, σ_e is electrical conductivity, κ is thermal conductivity, and T is temperature. The electronic charge carriers that are required for an optimum zT is often provided by the intrinsic defects in superionic materials. For instance, an off-stoichiometry of $x = 0.01$ in $Cu_{2-x}Se$ provides p-type carriers at a level of $n \approx 2 \times 10^{20}$ /cm^{-3}, which is close to the optimum level for high temperature performance.

Copper (I) selenide is one of the special cases of superionic materials, where promising behavior is found not just in its superionic phase at high temperature, but also at the superionic phase transition [8, 9]. The phase transition of $Cu_{2-x}Se$ from its room temperature phase (α) to the superionic high temperature phase (β) accompanies drastic changes in the electronic and thermal transport properties (figures 1(a)–(c)), in addition to the orders of magnitude increase in ionic conductivity that characterizes superionic transitions [10]. The thermopower increases super-linearly (figure 1(a)); both the electrical and thermal diffusivity plunge (figures 1(b)–(c)). As a combined result, the figure-of-merit for thermoelectric performance improves by two- [8] or seven-fold [9] around the transition (figure 1(d)), depending on how one converts the measured thermal

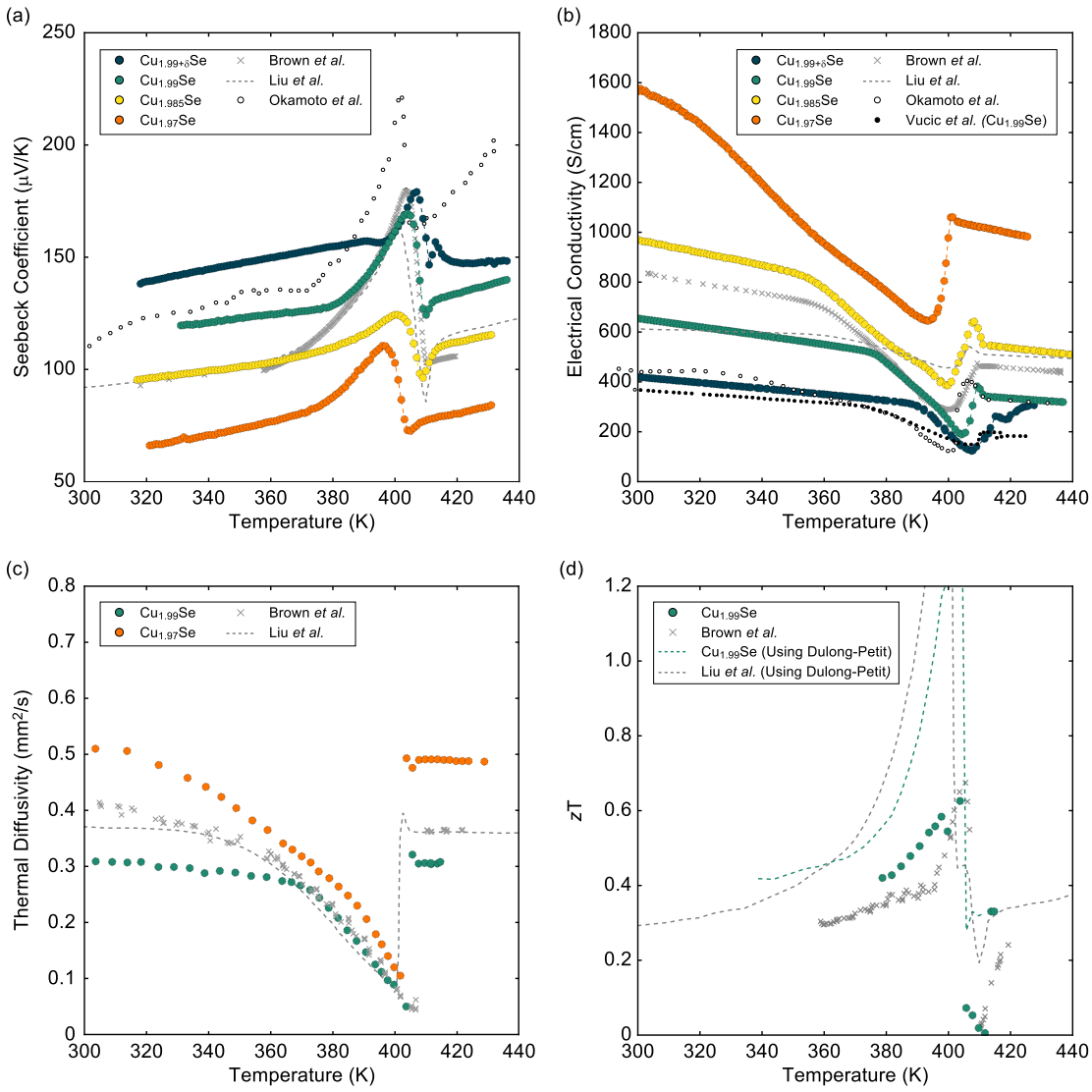

Figure 1. Transport properties of $Cu_{2-x}Se$ around the superionic phase transition. (a) Seebeck coefficient (b) electrical conductivity (c) thermal diffusivity (d) thermoelectric figure-of-merit. The dashed lines in zT are estimates that result from using the Dulong–Petit baseline for heat capacity. Colored circles in all sub-figures are data from this study. Literature data [8, 9, 11, 12] all report a nominal composition of Cu_2Se unless otherwise specified. All data from this study are measured upon heating.

diffusivity to thermal conductivity. This conversion depends on the interpretation of heat capacity measurements, which in turn relies on how the phase transition is understood.

The drastic changes in properties near the phase transition has been attributed to critical fluctuations by a number of studies [8, 9, 13–15] and has been considered a potentially new mechanism for enhancing thermoelectric performance. Brown *et al* has suggested a coupling between critically increased entropy and charge transport, resulting in 'additional thermopower' that increases with a power law near the transition [8]. Liu *et al* has also argued that critical scattering provides a significant advantage [9]. Mahan has modeled the increase in thermopower with an exponentially increased broadening in the electronic states and suggested its relation to critical fluctuations [13]. These arguments have been partly supported by the λ-like peak in heat capacity [8, 14], which is typically associated with critical fluctuations inherent in continuous phase transitions. A gradual evolution in the x-ray powder diffraction pattern [8, 9, 14] and also the NMR signal [15] has also been considered a signature for a continuous phase transition.

However, as will be shown in this paper, symmetry restrictions disallow this phase transition to be continuous. In addition, many experimental indications such as the strong hysteresis with temperature [16] has been overlooked. These points altogether suggests that the transport property behavior at the $Cu_{2-x}Se$ superionic phase transition should be explained with a discontinuous transition picture rather than with critical fluctuations. In light of this understanding, we refer to the drastic changes associated with the phase transition as

'apparent critical behavior'. In this paper, we show that compositional degree of freedom can cause apparent signatures that look similar to what might be associated with critical behavior.

2. Review of the atomic and electronic structures

We first briefly review some basic properties of the room temperature phase (α) and high temperature phase (β) of $Cu_{2-x}Se$. The β phase has an average structure similar to the antifluorite structure (space group $Fm\bar{3}m$). The Se anions occupy the 4a sites with a face-centered cubic arrangement, while the Cu cations are disordered throughout the lattice occupying tetrahedral 8c and trigonal 32f sites in a split atom model [17]. The cation disorder is dynamical in nature as evidenced by the inelastic signal probed in diffraction experiments [18]. The α phase is a superstructure of the β phase where the cations are ordered. Some monoclinic [19, 20] or triclinic [21] models have been proposed, but a complete model has not yet been determined. This uncertainty remains as a difficulty in understanding experimental results.

Electronically, both α and β phases are semiconductors with a band gap. In the α phase, an optical band gap of 1.23 eV has been measured by room temperature optical absorption [22]. The chemical potential is determined by the Cu vacancy concentration, typically positioned near the valence band edge for small x. For instance, a sample with room temperature thermopower of 100 μV K^{-1} would indicate a chemical potential 0.06 eV into the valence band within a parabolic dispersion assumption. An increase in Cu vacancies (or the off-stoichiometry x) would further shift the chemical potential into the valence band. The β phase is also believed to be a semiconductor with a finite gap, despite some calculations [21, 23] on the antifluorite structure predicting a zero gap feature. Transport measurements do not show any signs of gap closing.

3. Violation of Landau's criteria

Landau's necessary condition for continuous phase transitions can be used to see if it is possible for a given transition to be continuous [24]. This condition comes from Landau's expansion of the free energy in terms of order parameters:

$$\Phi(P,\ T;\ \eta) = \Phi_0 + A(P,\ T)\cdot\eta^2 + B(P,\ T)\cdot\eta^3 + C(P,\ T)\cdot\eta^4, \tag{2}$$

where Φ is Landau's free energy and η is the order parameter(s). The coefficient of the second order term determines the phase boundaries in the P–T plane: $A(P,\ T) = 0$. The coefficient of the third order term provides the necessary condition for a continuous transition, where continuity of the transition requires $B(P,\ T) = 0$. This condition for continuity is of interest in the current case.

In order-disorder structural transitions, this necessary condition for a continuous transition can be readily tested by looking at the 'concentration waves' which is a well established method from metallurgy [25, 26]. Concentration waves are ordering vectors that can be found by observing the super lattice reflection peaks in diffraction experiments. In the current case of $Cu_{2-x}Se$, electron diffraction studies [19, 27] have identified $\left(0\frac{2}{3}\frac{2}{3}\right)$-type vectors. The collection of these ordering vectors, $\{\mathbf{k}_0\}$, includes all that are generated from the symmetry of the disordered phase if those generated are unique vectors.

The condition that is equivalent to $B(P,\ T) = 0$ in order-disorder transitions is when not *any* three unique ordering vectors from $\{\mathbf{k}_0\}$ add up to a reciprocal lattice vector ($\mathbf{G}$):

$$\mathbf{k}_{0,i} + \mathbf{k}_{0,j} + \mathbf{k}_{0,k} \neq \mathbf{G}. \tag{3}$$

In $Cu_{2-x}Se$, we can find many combinations from $\{\mathbf{k}_0\}$ such as:

$$\left(0\frac{2}{3}\frac{2}{3}\right) + \left(\frac{2}{3}0\frac{\bar{2}}{3}\right) + \left(\frac{\bar{2}}{3}\frac{\bar{2}}{3}0\right) = (000) \tag{4}$$

that sufficiently determines the phase transition to be first order. In the following sections, we show how experimental observations can indeed be well explained by assuming a first order phase transition.

4. Experimental methods

4.1. Materials synthesis

$Cu_{2-x}Se$ samples were prepared by reacting stoichiometric amounts of Cu and Se shots (Alfa Aesar, 99.999% on a metals basis). Prior to the reaction, the Cu shots were further reduced in a 1% H_2–99% Ar atmosphere at 700 °C. We find this reduction a crucial step for precise control on the stoichiometry of the sample. The elements were placed in carbon-coated silica ampoules in an Ar-filled glove box and sealed under vacuum at $<1 \times 10^{-4}$ torr. The elements were melted at 1170 °C for 12 h, subsequently annealed at 700 °C for 72 h, and

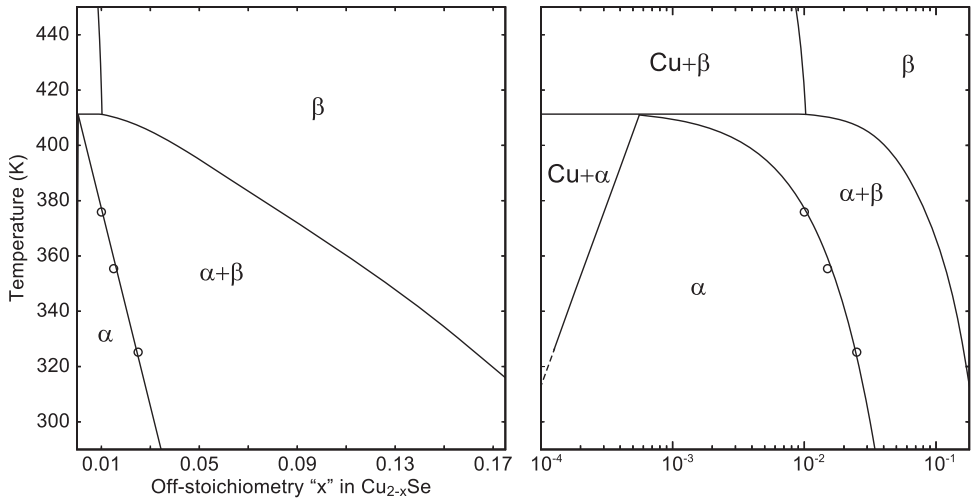

Figure 2. The phase diagram of the peritectoid $Cu_{2-x}Se$ system, drawn with the composition in linear (left) and log (right) scale. The phase boundaries are after [27, 29]. The open circles represent the kink positions observed from the electrical conductivity measurements (figure 1(b)).

slowly cooled to room temperature. The ingots were ball-milled under Ar atmosphere to produce powder. The powder samples were transferred into 0.5 inch diameter high density graphite dies and were consolidated into 1–2 mm thick pellets by hot-pressing at 700 °C for 1 h under Ar atmosphere and a pressure of 45 MPa. The density of the pellets was typically ≈ 6.7 g cm^{-3}.

4.2. Measurement of transport properties

The electrical conductivity was measured with a van der Pauw four-probe method while heating under vacuum (6 K h^{-1}). The thermopower was measured under vacuum with a two-probe configuration of Chromel/Nb thermocouples, using an apparatus described in [28]. To obtain data points with small temperature steps while maintaining a well-defined heating rate, the temperature was ramped linearly (25 K h^{-1}) with a fixed temperature difference between the two sides of the sample. After a number of cycles with different temperature gradients, the data points from each temperature were collected and linearly fitted to yield the Seebeck coefficient. The thermal diffusivity was measured using the laser flash method with a Netzsch LFA 457 instrument.

5. The phase diagram of $Cu_{2-x}Se$

Determining the relevant phase diagram of $Cu_{2-x}Se$ is central to understanding the phase transition behavior. Drawn in figure 2 is the phase diagram of $Cu_{2-x}Se$, mostly determined by Ishikawa *et al* [29], which we find to be most consistent with experimental observations. Particularly, in between the room temperature phase (α) and high temperature phase (β), we note the existence of a phase-mixture region ($\alpha + \beta$) which has been evidenced by diffraction—peaks characteristic of each phase are found to coexist (see section 6.4). Any path on the phase diagram that crosses through this phase mixture region would then undergo a transformation with a composition shift in each phase and change in phase fractions, over an extended temperature range. The phase coexistence over a temperature range is actually an indication of a 1st order phase transition [24]. The existence of other single phase regions between α and β as suggested in [27] is not possible on this phase diagram once we acknowledge the phase mixture region, since a new single-phase region should only meet with the two-phase region at one point on the phase diagram according to the Gibbs phase rule.

We remind that the composition of the samples which show apparent critical behavior (shown in figure 1) all correspond to $Cu_{2-x}Se$ with an off-stoichiometry as high as $x \approx 0.04$. The off-stoichiometry can be approximately inferred from the room temperature Hall carrier concentration of holes, which amounts to $n_H \approx 2 \times 10^{20}$/cm^3 for the case of $Cu_{1.99}Se$. All samples shown in figure 1 have a Hall carrier concentration of a comparable order of magnitude, despite some them often being reported with a nominal composition of Cu_2Se (see figure 1 caption). In other words, all of these samples cross a phase mixture region according to the phase diagram shown in figure 2, which we find to be the essence in explaining the apparent anomalous features. In the following section, we show that the phase diagram shown in figure 2 well explains the experimental observations.

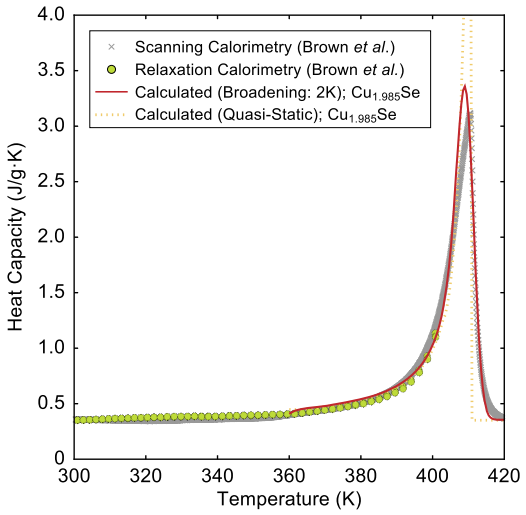

Figure 3. Heat capacity of $Cu_{1.985}Se$. Gray crosses are data measured with differential scanning calorimetry and brown solid-circles are from relaxation calorimetry, both after [8]. The sample composition corresponding to this data was inferred from the transition onset temperature shown from transport measurements (see figure 1). The dashed line shows the calculated heat capacity of this composition based on the phase diagram shown in figure 2, and by assuming a broadening of 2 K. The calculated curve with no broadening (quasi-static) is shown with the dotted line.

6. The apparent critical behavior

6.1. Heat capacity

It is common to associate a λ-shape peak in the heat capacity with a continuous phase transition since it implies the existence of critical fluctuations; however, peaks that look similar to a λ-shape can result from other reasons as well. In the case of $Cu_{2-x}Se$, the apparent λ-shape peak in the heat capacity curve is accounted for by recognizing that transformation enthalpy is continuously distributed over an extended temperature range because the phase fractions gradually change while crossing the phase mixture region. This case is in contrast to 1st order transitions in single component systems where the transformation enthalpy is a delta function at a single temperature. By knowing the total transformation enthalpy of $Cu_{2-x}Se$ ($\approx$30 J g^{-1}), the phase diagram allows to calculate the heat capacity curve with the assumption that the transformation enthalpy is insensitive to the composition in this small off-stoichiometry range. The result, shown in figure 3, agrees well with the measurement.

We see from the agreement that a λ-shape peak does not necessarily indicate a continuous phase transition; the compositional degree of freedom allows gradual transformation over an extended temperature range, and the large transformation enthalpy of the superionic phase transition makes this feature prominent in heat capacity. In fact, similar cases can be found when melting peritectic alloys [30–32]. In such cases the material goes through partial melting over a temperature range with a large fusion enthalpy. Note that fusion enthalpy is comparable to superionic transition enthalpy when scaled with temperature and atomic fraction (consistent with the term 'sublattice melting of the cations'), and thus both cases appear prominently in heat capacity measurements.

6.2. Electrical conductivity

The plunge in electrical conductivity upon heating throughout the transformation can be understood as a result of hole carriers depleting in the main phase (α). The kinks at the onset of a slope change in electrical conductivity against temperature (see arrows in figure 4) correspond to the α phase boundary (figure 2). According to the phase diagram, the composition of the α phase will follow the phase boundary where the concentration of Cu vacancies decreases linearly upon heating. Since each Cu vacancy provides approximately one hole carrier, the charge carrier concentration in the main phase would decrease linearly, hence the linear decrease in conductivity. The secondary phase (β) nucleates with a higher amount of Cu vacancies, and thus has a higher electrical conductivity. As β phase becomes the main phase, the conductivity trend turns over until the system moves into to the single phase region of β.

The electrical conductivity curves of this phase mixture can be calculated using effective medium theory. From the single phase temperature regions (below and above the dip), we use the Drude relation $\sigma = ne\mu$ to extract the temperature dependent mobility μ since the carrier concentration n is fixed by the off-stoichiometry in this region. In the phase mixture region, we assume that the phase fractions and respective compositions

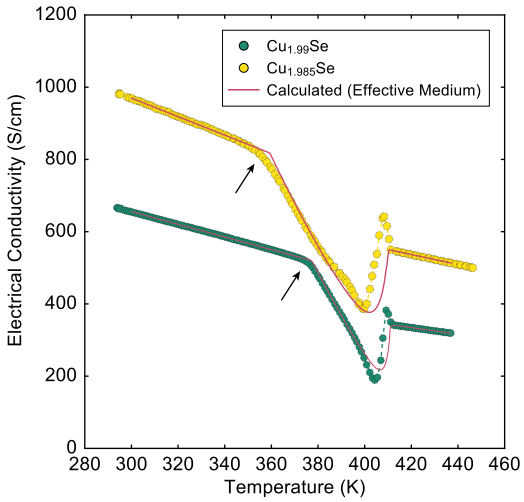

Figure 4. The change in electrical conductivity explained by taking into account the two-phase region in the phase diagram. Red solid lines represent the calculated result from effective medium theory as in equation (5). Data were measured upon heating with a rate of 6 K h^{-1}. The kinks in the curve marked with arrows indicate the onset of the phase transformation.

follow the phase diagram (figure 2). We estimate the conductivity of each phase constituent by using these compositions from the phase diagram, which determines the carrier concentration. To get the overall conductivity of the medium, we use the effective medium theory for spherical grains [33]:

$$\sum_i f_i \frac{\sigma_i - \sigma_m}{\sigma_i + 2\sigma_m} = 0, \tag{5}$$

where f_i and σ_i are the fraction and conductivity of constituent phases, respectively. σ_m gives the self-consistent solution which is the effective medium value. Figure 4 shows good agreement with the measurement. Note that no fitting parameters were introduced in this calculation. The minor disagreement is believed to be mostly associated with the uncertainty of the phase diagram and ignorance of the microstructural details. Further information about the microstructure could refine the calculation [34]. We note that our explanation for conductivity is in parallel with one of the earliest studies by Ogorelec *et al* [35].

6.3. Seebeck coefficient

The thermopower change during the phase transformation can be understood with the same framework as that for electrical conductivity: carrier concentration decrease in the main phase leads to an initial increase in thermopower until it is turned over by the new superionic phase. The thermopower curves shown in figure 1(a) are qualitatively an inverse of the electrical conductivity curves shown in figure 1(b).

Previously, it was suggested that there is 'additional thermopower' at the superionic phase transition by comparing the measured thermopower and estimated thermopower based on Hall measurements and an effective band model [8]. However, we find that a phase mixture ($\alpha + \beta$) following the phase diagram permits a thermopower with an upper bound that is higher than what is measured. To estimate the bounds of the phase mixture, we first estimate the transport properties of the constituent phases at each temperature. First, electrical conductivity can be calculated as described in the previous section. Second, the thermopower of each phase can be estimated by scaling the measured values from the single phase region, where the scaling is determined by the change in electrical conductivity. The measured thermopower serves as a reference that allows to infer the position of the reduced chemical potential $\eta = (\mu - E_c)/kT$ through:

$$S = \frac{k}{q}\left(\frac{2F_1(\eta)}{F_0(\eta)} - \eta\right), \tag{6}$$

where μ is the chemical potential, E_c is the band edge position, k is the Boltzmann constant, q is the charge of the carrier, and F_i is the complete Fermi–Dirac integral of i'th order. Then, knowing how η changes when the temperature moves into the phase mixture region would allow to estimate how the thermopower changes. Change in electrical conductivity provides this information:

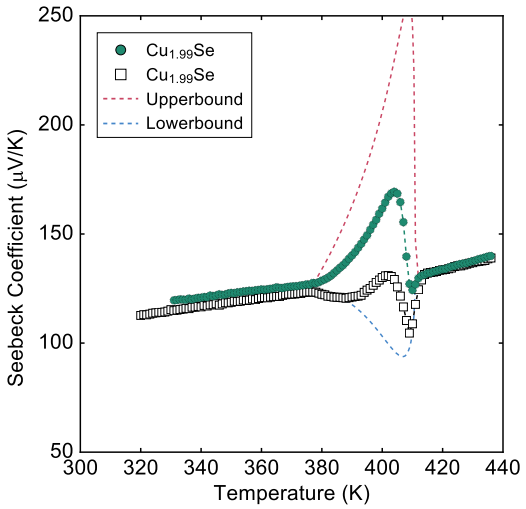

Figure 5. The measured thermopower values are within the bounds of what is permitted by a two-phase mixture. The color-circled points represent the behavior that was most often observed from $Cu_{1.99}Se$ samples. The white-squared points show an occasional case when a different transition curve was observed with the same sample but during a different round of measurement . With each setup, the measurement was cycled a number of times with consistent behavior. Dashed lines show the calculated upper (red) and lower (blue) bounds of thermopower from an effective medium of a two-phase mixture [34]. The bounds represent two opposite extremes of the microstructure, and an arbitrary microstructure results in a curve within these bounds. All data points were obtained upon heating.

$$\frac{\sigma_i}{\sigma_f} = \frac{F_0(\eta_i)}{F_0(\eta_f)}, \tag{7}$$

where subscripts denote an arbitrary temperature point. This equation can be derived from the assumption of acoustic phonon scattering where conductivity depends on temperature only through $\sigma \propto F_0(\eta)$ [36]. Third, for thermal conductivity, we use the lattice thermal conductivity value estimated from the single phase region and assume this value as constant for each phase throughout the temperature range of interest. We add the electronic contribution using the information of thermopower and conductivity. With these transport properties of the constituent phases, the upper and lower bounds of the phase mixture can be calculated with effective medium theory (equations (62) and (63) from [34]). In the current case, the upper bound corresponds to one extreme of the microstructure where two phases are in a series circuit configuration. The calculation results (figure 5) show that the measured thermopower is well below this upper bound. The actual manifest of thermopower from the phase mixture medium is highly dependent on the actual microstructure. For example, the other extreme of effective medium, a parallel circuit configuration, rather predicts a decrease in thermopower. In fact, samples with the same composition do occasionally show significant variations in the transition curve despite having similar Seebeck coefficients above and below the transition. Precisely reproducing the measured thermopower would require specific information about the microstructure evolution of the phase mixture, which is beyond the aim of this study. Nevertheless, the effective medium bound shows that the steep increase in thermopower can be explained without introducing additional mechanisms or sources of thermopower.

6.4. Diffraction peaks

The gradual change in peak positions and intensity (figure 6 and [8, 9, 14]), rather than an abrupt change, of the powder diffraction pattern during the phase transformation is another feature that has previously been suggested as evidence for a continuous phase transition [8, 9]; however, the gradual change in phase fraction while crossing the phase mixture region of the phase diagram (figure 2) would also result in such a gradual evolution in the powder diffraction pattern since the peak intensity is proportional to the phase fraction. In addition, changes in phase fraction accompany composition change in the individual phases, which induces a shift in the peak positions. For example, as the composition gets closer to the stoichiometric ratio, the peaks of the β phase shift to a smaller angle due to lattice expansion [37]. Such trends are noticeable in the data shown in [9].

Specific diffraction peaks continuously decaying to zero intensity is not a feature exclusive to near-continuous phase transitions when there is compositional degree of freedom in the system. What rather matters is that there are diffraction peaks characteristic to each phase (e.g. peak at $Q = \frac{4\pi \sin\theta}{\lambda} \approx 0.9$, 2.75 and 4.1 Å^{-1} for the α phase and $Q \approx 2.15$ Å^{-1} for the β phase), and also that they coexist at a range of temperatures

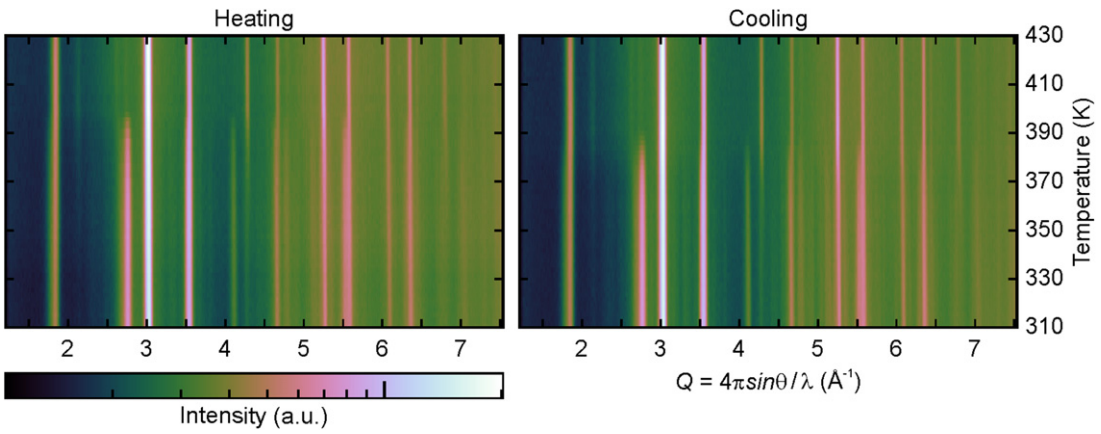

Figure 6. Powder diffraction patterns of $Cu_{1.985}Se$ obtained by neutron diffraction in the phase transition temperature range. The gradual change in peak intensities is a result of the continuous change of phase fractions. Hysteresis can be seen by comparing the temperatures at which peaks decay and grow, which is a strong indication of a discontinuous phase transition. Phase coexistence during the transformation is manifested by the temperature overlap of α and β phase peaks (e.g. $Q \approx 2.75$ and 2.15 $Å^{-1}$ for α and β, respectively). The brightness of the color is proportional to the logarithm of the intensity. The data were collected with the Wombat neutron diffractometer at the OPAL reactor of ANSTO using a wavelength of 1.544 Å. The sample was loaded in a cylindrical vanadium container, and the measurements were done at fixed temperatures with a 1 K increment.

(figure 6 and [38]). Such features indicate a 1st order transition and also a phase mixture region. Contradictory interpretations in the literature can be partly attributed to the incomplete understanding of the α phase crystal structure (e.g. the structural model for the α phase [20] does not agree with the measured pair distribution function [8]) and also the large diffuse background signal [18, 38], which limits quantitative analysis of the diffraction patterns.

We note that Danilkin *et al* has recently found Cu cation ordering upon cooling a single crystal of pure β phase (estimated composition $Cu_{1.85}Se$) that seems to lead to a phase transition to an ordered β' phase [39]. By tracking the temperature dependent elastic component of the intensity of a $\left(\frac{1}{2}\frac{1}{2}\frac{1}{2}\right)$-type superlattice reflection, a growth from zero intensity at 350 K with a power law agreeing with the 3D Ising model was shown. This observation could possibly indicate a continuous phase transition such as $\beta \rightarrow \beta'$. However, this cation ordering in the superionic β phase is unrelated to the apparently anomalous behavior described in the previous sections since the β' phase is distinct from the α phase. This ordering seems to rather manifest when the transition to α is not favored until lower temperatures, which is possible for compositions close to $Cu_{1.8}Se$. Such observations could indicate that the β phase boundary bordering the $\alpha + \beta$ phase region drawn in figure 2 might have to be shifted towards the Cu-rich side in order to accommodate a β' phase region.

6.5. Figure-of-merit

The increase in zT around the phase transition can be understood as a result of the electric charge carrier concentration of the α-phase being tuned towards the optimum for thermoelectric performance. As shown in figure 7, the carrier concentration (or chemical potential) of $Cu_{1.99}Se$ is higher than the optimum level. As the material transforms to a phase-mixture upon increasing the temperature, the carrier concentration of the α-phase decreases (chemical potential moves closer to the band edge) because of the composition shift, leading to a level near the optimum. The maximum possible zT of the phase-mixture is bounded by the maximum of the superior phase [34] (α-phase in this case), while the zT actually observed is deteriorated due to the β-phase which has a carrier concentration higher than the optimum by an order of magnitude.

7. Implications for thermoelectrics

One immediate interest for thermoelectrics regarding the superionic phase transition of $Cu_{2-x}Se$ is the correct estimation of the figure-of-merit zT defined by equation (1). Discrepant estimations for zT stem from converting the measured thermal diffusivity D to thermal conductivity $\kappa = D\rho C_p$, where C_p is the heat capacity and ρ is density. Quoting a low heat capacity can result in an underestimated thermal conductivity, and therefore a zT that is proportionally higher. In one report [9], the baseline heat capacity was used instead of the measured value from the heat capacity peak, resulting in $zT \approx 2.3$. The rationale behind this would be assuming a 1st order transition that happens at a single temperature, and thus assuming that the measured peak in heat capacity

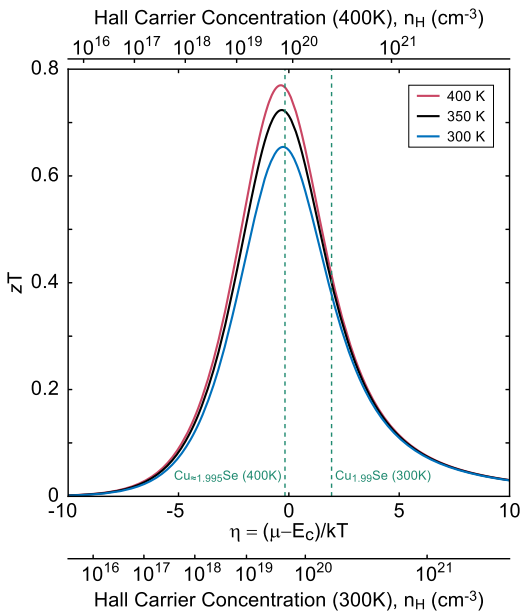

Figure 7. The zT curve of α–$Cu_{2-x}Se$ with respect to the reduced chemical potential, η. The η of $Cu_{1.99}Se$ at 300 K, which corresponds to $n_H = 2.08 \times 10^{20}$ cm^{-3} (measured), is away from the thermoelectric optimum. At 400 K, an overall composition of $Cu_{1.99}Se$ is a phase-mixture with the α-phase being approximately $Cu_{1.995}Se$. This composition would have η positioned near the optimum, yielding a maximum $zT \approx 0.75$, which also determines the the upper limit of the $\alpha + \beta$ phase mixture.

is actually a delta function at the transition temperature. On the other hand, a different report [8] has assumed a continuous transition, where the measured heat capacity values are considered quasi-static values that would result from critical fluctuations; the estimation of the peak zT was ≈0.7. Analogous issues arise in other similar systems such as $Cu_{2-x}S$ [3].

According to our interpretation, the increased heat capacity from the broad peak, rather than that from the baseline, is the relevant value despite the phase transition being 1st order. The transformation enthalpy is not a delta function in temperature, but is a distributed function with a shape that reflects the phase boundaries in the phase diagram. Accordingly, the heat capacity departs from the baseline due to this transformation enthalpy distributed in a temperature range. While the quasi-static heat capacity is determined by the phase diagram, the effective heat capacity relevant for transient measurements such as laser flash diffusivity measurements is a more complicated issue. Nevertheless, the fact that scanning and relaxation calorimetry show agreement (figure 3) and also that these values are consistent with the values inferred by comparing diffusivity and effusivity measurements [40], altogether suggest that usage of the quasi-static heat capacity yields a fair estimation for thermal conductivity and zT. Furthermore, it has been shown from laser flash measurements of a peritectic phase mixture that the baseline heat capacity is not relevant in deducing thermal conductivity [30]. Our estimation for zT of $Cu_{1.99}Se$ at the transition is shown in figure 1(d), with a peak value smaller than 0.75.

Another interest for thermoelectrics is whether this phase transition bears any general significance. One notable feature of this phase transition is that it shows a mechanism of how a material system can inherently tune its carrier concentration towards a lower value with increasing temperature. Such a mechanism is required to reach self-compatibility in thermoelectric cooling, referred to as 'Thomposon coolers' to distinguish with conventional Peltier coolers where material performance is only optimal at a local region within the material [41]. If a material system with similar self-tuning behavior and also maximum zT in the tuning region could be found, it would be able to achieve Thompson cooling. Materials with superionic phase transitions could be good candidates because the high entropy associated with cations tend to provide extended phase widths that could produce similar phase change behavior. In addition, superionic materials in general have low thermal conductivity and fast transformation kinetics.

On the other hand, we do not find any evidence for enhanced zT or thermopower that is associated with critical behavior. The transport properties are well explained by assuming a classical phase mixture that behaves following the phase diagram shown in figure 2. The enhancement in zT can be understood as a result of the carrier concentration in the main phase (α) being tuned towards the optimum for the transition temperature.

8. Conclusions

The superionic phase transition of $Cu_{2-x}Se$ accompanies drastic changes in transport properties. In contrast to previous suggestions about critical behavior, we find that the experimental observations are rather a result of an extended phase mixture region. The phase diagram that depicts this phase mixture is consistent with a discontinuous phase transition, as predicted by Landau's criteria. Many apparent signatures of a continuous transition can be explained by a continuous change in the phase fractions.

Acknowledgments

The authors thank Prof Peter W Voorhees for his insightful comments and ANSTO (Australia) for the provision of beam time. UA acknowledges the financial assistance from The Scientific and Technological Research Council of Turkey. The work conducted at Caltech was supported by the AFOSR MURI program under FA9550-12-1-0002. The work conducted at Northwestern University was supported by the Solid-State Solar-Thermal Energy Conversion Center, an Energy Frontier Research Center funded by the U.S. Department of Energy, Office of Science, Basic Energy Sciences (#DE-SC0001299).

References

[1] Liu H, Shi X, Xu F, Zhang L, Zhang W, Chen L, Li Q, Uher C, Day T and Snyder G J 2012 *Nat. Mater.* **11** 422
[2] Yu B, Liu W, Chen S, Wang H, Wang H, Chen G and Ren Z 2012 *Nano Energy* **1** 472
[3] He Y, Day T, Zhang T, Liu H, Shi X, Chen L and Snyder G J 2014 *Adv. Mater.* **26** 3974
[4] Snyder G J, Christensen M, Nishibori E, Caillat T and Iversen B B 2004 *Nat. Mater.* **3** 458
[5] Ballikaya S, Chi H, Salvador J R and Uher C 2013 *J. Mater. Chem.* A **1** 12478
[6] Boyce J B and Huberman B A 1979 *Phys. Rep.* **51** 189
[7] Snyder G J and Toberer E S 2008 *Nat. Mater.* **7** 105
[8] Brown D R, Day T, Borup K A, Christensen S, Iversen B B and Snyder G J 2013 *APL Mater.* **1** 052107
[9] Liu H *et al* 2013 *Adv. Mater.* **25** 6607
[10] Horvatic V and Vucic Z 1984 *Solid State Ion.* **13** 117
[11] Okamoto K 1971 *Japan. J. Appl. Phys.* **10** 508
[12] Vucic Z, Horvatic V and Ogorelec Z 1982 *J. Phys. C: Solid State Phys.* **15** 3539
[13] Mahan G D 2015 *J. Appl. Phys.* **117** 045101
[14] Liu H, Shi X, Kirkham M, Wang H, Li Q, Uher C, Zhang W and Chen L 2013 *Mater. Lett.* **93** 121
[15] Sirusi A A, Ballikaya S, Uher C and Ross J H 2015 *J. Phys. Chem.* C **119** 20293
[16] Chrissafis K, Paraskevopoulos K M and Manolikas C 2006 *J. Therm. Anal. Calorimetry* **84** 195
[17] Skomorokhov A N, Trots D M, Knapp M, Bickulova N N and Fuess H 2006 *J. Alloys Compd.* **421** 64
[18] Danilkin S A 2009 *J. Alloys Compd.* **467** 509
[19] Milat O, Vucic Z Z and Ruscic B 1987 *Solid State Ion.* **23** 37
[20] Gulay L, Daszkiewicz M, Strok O and Pietraszko A 2011 *Chem. Met. Alloys* **4** 200
[21] Kashida S, Shimosaka W, Mori M and Yoshimura D 2003 *J. Phys. Chem. Solids* **64** 2357
[22] Sorokin G P, Papshev Y M and Oush P 1966 *Sov. Phys. Solid State* **7** 1810
[23] Rasander M, Bergqvist L and Delin A 2013 *J. Phys.: Condens. Matter* **25** 125503
[24] Landau L D and Lifshitz E M 1980 *Statistical Physics Part 1* 3rd edn rev (Oxford: Pergamon)
[25] Khachaturyan A G 1978 *Prog. Mater. Sci.* **22** 1
[26] De Fontaine D 1979 Configurational thermodynamics of solid solutions *Solid State Physics* vol 34 (New York: Academic) pp 73–274
[27] Vucic Z, Milat O, Horvatic V and Ogorelec Z 1981 *Phys. Rev.* B **24** 5398
[28] Iwanaga S, Toberer E S, LaLonde A and Snyder G J 2011 *Rev. Sci. Instrum.* **82** 063905
[29] Ishikawa T and Miyatani S-y 1977 *J. Phys. Soc. Japan* **42** 159
[30] Monaghan B J, Neale J G J and Chapman L 1999 *Int. J. Thermophys.* **20** 1051
[31] Wallbrecht P C, Blachnik R and Mills K C 1981 *Thermochimica Acta* **45** 189
[32] Wallbrecht P C, Blachnik R and Mills K C 1981 *Thermochimica Acta* **46** 167
[33] Landauer R 1952 *J. Appl. Phys.* **23** 779
[34] Bergman D J and Levy O 1991 *J. Appl. Phys.* **70** 6821
[35] Ogorelec Z and Celustka B 1969 *J. Phys. Chem. Solids* **30** 149
[36] Fistul V I 1969 *Heavily Doped Semiconductors* (New York: Plenum) ch 3
[37] Danilkin S A, Avdeev M, Sale M and Sakuma T 2012 *Solid State Ion.* **225** 190
[38] Danilkin S A, Avdeev M, Sakuma T, Macquart R and Ling C D 2011 *J. Alloys Compd.* **509** 5460
[39] Danilkin S A, Kearley G J, Deng G, Avdeev M, Yu D, Liu H, Shi X, Chen L D, Pomjakushina E and Sakuma T 2015 *34th Annual Int. Conf. on Thermoelectrics*
[40] Brown D R, Heijl R, Borup K A, Iversen B B, Palmqvist A and Snyder G J 2016 in preparation
[41] Snyder G J and Ursell T S 2003 *Phys. Rev. Lett.* **91** 148301